International Journal of Remote Sensing

ISSN: 0143-1161 (Print) 1366-5901 (Online) Journal homepage: https://www.tandfonline.com/loi/tres20

Species stratification and upscaling of forest carbon estimates to landscape scale using GeoEye-1 image and lidar data in sub-tropical forests of Nepal

Pema Wangda, Yousif A. Hussin, M.C. Bronsveld & Yogendra K. Karna

To cite this article: Pema Wangda, Yousif A. Hussin, M.C. Bronsveld & Yogendra K. Karna (2019) Species stratification and upscaling of forest carbon estimates to landscape scale using GeoEye-1 image and lidar data in sub-tropical forests of Nepal, International Journal of Remote Sensing, 40:20, 7941-7965, DOI: 10.1080/01431161.2019.1607981

To link to this article: https://doi.org/10.1080/01431161.2019.1607981

INTERNATIONAL JOURNAL OF REMOTE SENSING
2019, VOL. 40, NO. 20, 7941–7965
https://doi.org/10.1080/01431161.2019.1607981

Taylor & Francis
Taylor & Francis Group

Species stratification and upscaling of forest carbon estimates to landscape scale using GeoEye-1 image and lidar data in sub-tropical forests of Nepal

Pema Wangda[a], Yousif A. Hussin[b], M.C. Bronsveld[b] and Yogendra K. Karna[c]

[a]Renewable Natural Resources Statistics Division, GIS and Remote Sensing Section, Ministry of Agriculture and Forests, Thimphu, Bhutan; [b]Department of Natural Resources, Faculty of Geo-information and Earth Observation (ITC), University of Twente, Enschede, The Netherlands; [c]School of Ecosystem and Forest Sciences, The University of Melbourne, Creswick, Australia

ABSTRACT

Aboveground forest biomass and carbon estimation at landscape scale is crucial for implementation of REDD+ programmes. This study aims to upscale the forest carbon estimates using GeoEye-1 image and small footprint lidar data from small areas to a landscape level using RapidEye image. Species stratification was carried out based on the spectral separability curve of GeoEye-1 image, and comparison of mean intensity and mean plot height of the trees from lidar data. GeoEye-1 image and lidar data were segmented using region growing approach to delineate individual tree crowns; and the segmented crowns (CPA) of tree were further used to establish a relationship with field measured carbon and total trees' height. Carbon stock measured from field, individual tree crown (ITC) segmentation approach and area-based approach (ABA) was compared at plot level using one-way ANOVA and *post hoc* Tukey comparison test. ITC-based carbon estimates was used to establish a relationship with spectral reflectance of RapidEye image variables (NDVI, RedEdge NDVI, PC1, single band of RedEdge, and NIR) to upscale the carbon at landscape level. One-way ANOVA resulted in a highly significant difference (p-value < 0.005) between the mean plot height and lidar intensity to stratify *Shorea robusta* and Other species successfully. ITC carbon stock estimation models of two major tree species explained about 88% and 79% of the variances, respectively, at 95% confidence level. The ABA estimated carbon was highly correlated (R^2 = 0.83, RMSE = 20.04) to field measured carbon with higher accuracy than the ITC estimated carbon. A weak relationship was observed between the carbon stock and the RapidEye image variables. However, upscaling of carbon estimates from ABA is likely to improve the relationship of the RapidEye variables rather than upscaling the carbon estimates from ITC approach.

ARTICLE HISTORY
Received 10 April 2018
Accepted 9 February 2019

1. Introduction

Forests play a crucial role in climate change adaptation and mitigation because they, as both carbon sources and sinks, have the potential to form an essential component

CONTACT Yogendra K. Karna ykarna@student.unimelb.edu.au School of Ecosystem and Forest Sciences, The University of Melbourne, Water St., Creswick, VIC 3363, Australia

in combating and mitigating global climate change. The Intergovernmental Panel on Climate Change (IPCC) has identified deforestation and forest degradation as a primary cause of greenhouse gas (GHG) emissions (IPCC 2007) in developing countries. Deforestation and forest degradation account for nearly 20% of global GHG emission, more than the entire global transport sector and second only to the energy sector (UNEP 2011). Therefore, reducing emissions from deforestation and forest degradation and enhancing the carbon stock is a crucial strategy to mitigate global climate change (Joseph, Sunderlin, and Verchot 2013). In 2008, the United Nations Framework Convention on Climate Change (UNFCCC) launched an initiative known as 'Reducing Emission from Deforestation and Forest Degradation (REDD)', whereby developing countries would be offered incentives to reduce emission from deforestation and increase carbon sequestration (UN-REDD 2011). By stimulating sustainable forest management practices in the existing forests as well as increasing the forest coverage, it is envisaged that REDD+ can increase the forest carbon stock and contribute significantly to the mitigation of global climate change. The UN-REDD + partner countries are required to develop cost-effective, robust, and compatible methods for estimation of carbon stock as a readiness requirement for the implementation of REDD+ (UN-REDD 2011). Nepal has strengthened its readiness for REDD + activities over the years with the submission of Readiness Preparation Proposal (R-PP), developing REDD+ Implementation Framework and Grievance Redressal Mechanism, developing forest measurement, reporting, and verification (MRV) and forest reference level (FRL) systems (MFSC 2018). However, one of the significant challenges for generating carbon incentives is the requirement of a transparent MRV system to estimate forest carbon stock accurately in a cost-effective manner (Bhattarai et al. 2015).

The principal element in the estimation of forest carbon stock is the measurement of forest biomass which includes aboveground (AGB) and belowground living mass, dead wood, and litter. Accurate aboveground biomass is estimated by harvesting the trees per unit area, oven drying and weighing them and then using allometric equations and modelling with a diameter at breast height (DBH) or in combination with tree height (Gibbs et al. 2007). These methods are laborious and impractical for application in large and inaccessible forest areas, while, remotely sensed data can be effective for forest inventory and biomass estimation to help in managing forests and ecosystem modelling (Yin and Wang 2016).

Remote sensing techniques in combination with ground-based measurements have been widely used to estimate forest biomass in a faster and cost-effective than traditional inventory methods (Gibbs et al. 2007). Several studies have been carried out to estimate forest biomass by using different ways and different sensors (Asner 2009; Johansen et al. 2007; Leckie et al. 2003; Muukkonen and Heiskanen 2007; Zheng et al. 2004; Lou et al. 2016; Karna et al. 2015). The use of coarse resolution satellite images such as NOAA-AVHRR, MODIS, etc. for biomass estimation is limited due to the occurrence of mixed pixels and inconsistent accuracy at regional or local scale (Patenaude, Milne, and Dawson 2005; Lu 2006). The use of moderate resolution satellite images (e.g. Landsat, ASTER) for AGB estimation is also confronted with the problem of mixed pixels (Muukkonen and Heiskanen 2007) and data saturation in complex biophysical environments (Lu 2006). Estimation of forest biomass and carbon stock using very high

resolution (VHR) satellite images such as QuickBird (Gonzalez et al. 2010; Leboeuf et al. 2007) and IKONOS (Song et al. 2010) improves the accuracy, but the frequent cloud cover and haze and smoke in the atmosphere limit acquisition of high quality satellite images in the tropical landscape.

Overall, the application of optical remote sensing for forest biomass estimation is limited to producing only 2-dimensional images, and it cannot represent the 3-dimensional spatial features of forests (Omasa et al. 2003; Gibbs et al. 2007). Light detection and ranging (lidar) has established itself as a standard technology for high resolution 3-dimensional topographic data acquisition in recent years as it has useful characteristics such as high sampling intensity, direct measurement of heights, precise geo-location, and automated processing for deriving forest biomass (Popescu 2007; Lin et al. 2017). lidar has been adopted by many studies (Lefsky et al. 1999a; Patenaude et al. 2004; Popescu 2007; Popescu, Wynne, and Scrivani 2004; Naesset 2011) for AGB estimation, as it offers substantial improvement in the accuracy of its prediction of forest attributes (Gonzalez et al. 2010; Lefsky, Cohen, and Spies 2001; Sexton et al. 2009). Furthermore, the integration of VHR satellite images and lidar provides more accurate AGB and carbon estimates than the stand-alone VHR, medium or coarse resolution satellite images (Lu 2006; Gibbs et al. 2007). Several studies have combined lidar and multispectral optical images for estimating forest structure attributes and obtaining more accurate results than using either lidar or optical images independently (Holmgren, Persson, and Soderman 2008; Ke, Quackenbush, and Im 2010; Leckie et al. 2003; Popescu, Wynne, and Scrivani 2004; Lou et al. 2016). Similarly, Rana et al. (2014) and Hou, Qing, and Tokola (2011) have used integrated remote sensing techniques; e.g. ALS, CIR aerial images and ALOS AVNIR-2 to assess above ground biomass in Asian tropical forests. However, drawbacks such as the need for large data storage, longer time for image processing (Ke and Quackenbush 2011a, 2011b), and data analysis and the high cost limit its application at a regional or national scale (Lu 2006) in developing countries. The accurate AGB and carbon estimates from the integration of VHR satellite image and lidar over smaller areas can be utilized as a reference data for estimating AGB and carbon at landscape level using medium resolution satellite images (Asner 2009; Gautam et al. 2010). Moreover, the upscaling of forest biomass and carbon from small areas to landscape level is a key research topic in forest biomass and carbon estimation studies (Shi and Liu 2017). Upscaling of biomass and carbon estimates by tree-centric approaches are less accurate (Coomes et al. 2017), but studies on the upscaling carbon estimates by species stratification using VHR and lidar in smaller areas to a landscape level are limited (Latifi et al. 2015). Therefore, the objective of this paper is to develop a methodology for upscaling the carbon estimates measured from individual tree crown segmentation method using VHR imagery and lidar data in smaller areas to a landscape level by using relatively coarser resolution satellite images such as RapidEye. In particular, this research used individual tree crown segmentation method for carbon estimation after stratification of tree species and compared it to the area-based approach of prior modelling and upscaling the carbon stock to landscape level.

2. Materials and methods

2.1. Study area

The study area is in the Ludhikhola watershed of Gorkha District of Nepal, located between 27°55′02″–27°59′43″N latitude and 84°33′23″–84°40′41″E longitude (Figure 1). Out of 31 community forests (CFs) with total area of 1888 ha, 5 CFs were selected for this study based on easy accessibility from the road point, availability of data, variation in terrain and representativeness of diverse forest structure types. The area represents a typical sub-tropical forest that was exposed to high deforestation and has been recently conserved through community forest management. It is characterized by an altitudinal variation and has upper tropical to sub-tropical lower forests. The forest comprises mixed forest with *Shorea robusta* (Sal) as the dominant tree species with a few other associated species like *Schiima wallichii, Rhus wallichii, Castanopsis indica, Terminalia alata*, etc.

2.2. Datasets

This study used a VHR GeoEye-1 satellite image with 2-m multispectral and 0.5-m panchromatic spatial resolution obtained on 2 November 2009 and a RapidEye satellite image with a spatial resolution of 5 m obtained on 22 April 2011. Small footprint airborne lidar data acquired between 16 March and 2 April 2011 using a Leica ALS-40 (Airborne Laser Scanner) sensor with an aerial platform flying at 2200 m with 80 knots flying speed and 52.9 kHz pulse rate. The lidar data was acquired at horizontal and

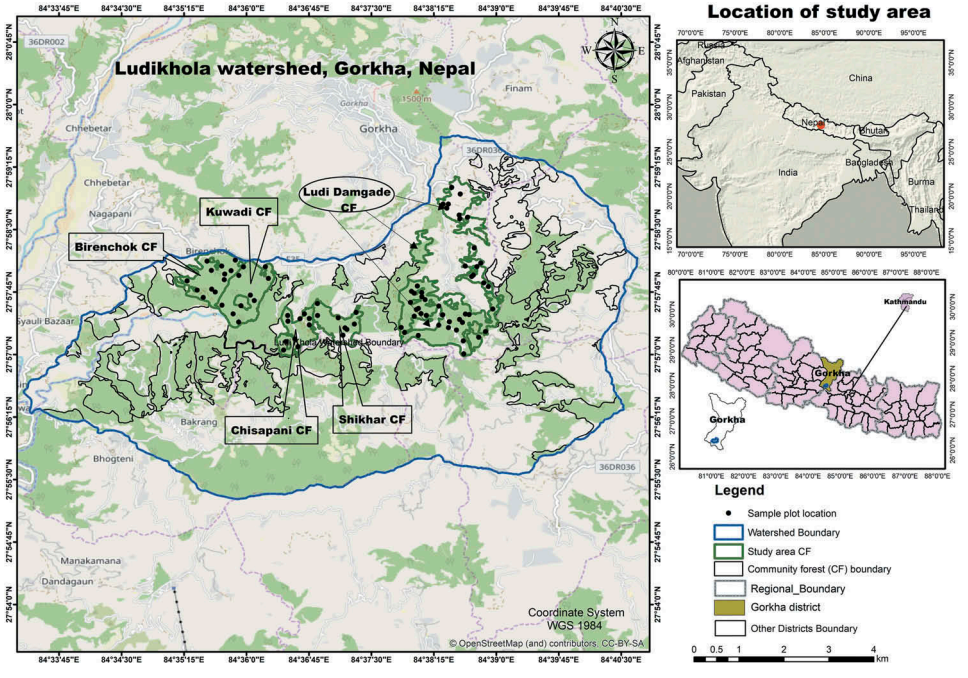

Figure 1. Location map of the study area.

vertical accuracies of 0.45 m each with an average point density of 0.8 points m^{-2} at the ground level.

Ground-based measurement of DBH, tree height, and crown diameter of each species was recorded in 84 sampling plots with the aid of a global positioning system (GPS) between 19 September and 20 October 2011. The data were collected for trees with DBH of 10 cm or more in a circular plot of 500 m^2 since trees with DBH less than 10 cm are assumed to contribute little to the total biomass of forest (Brown 2002). Circular plots are preferred in forest inventory as only a single dimension of the radius is required to define a parameter (Husch, Beers, and Kershaw 2003) and determination of tree inside circular plots is less problematic than other plot shapes. DBH was measured by diameter tape and the tree height by Trupulse 360B. Also, a total of 423 sample trees were identified on the printed GeoEye-1 image and the corresponding tree heights recorded to validate the tree heights derived from canopy height models (CHM). The methodological framework for this research is illustrated in Supplementary Figure 1.

2.3. Descriptive Statistics of field data

Forest stand parameters (DBH, height and crown diameter) were measured for 2793 trees with DBH above 10 cm in 84 sampling plots (71 *Shorea robusta* and 13 Other tree species) for all five community forests (CFs) covered by the study area. Forest inventory data revealed that a total of 27 different species were present in the study area and *Shorea robusta* was the dominant tree which constituted about 74% of the tree species. *Schima wallichii* constituted 12%, *Rhus wallichii* 3%, *Castanopsis indica* 3%, *Terminalia alata* 2%, and other species 6% of the tree species. The descriptive statistics of the DBH, height and crown diameter for *Shorea robusta* and Other tree species are presented in Table 1.

2.4. Aboveground biomass estimation from field data

Aboveground biomass was calculated using allometric equation (see Equation 1) with the field measured DBH and tree height. Since the species and site-specific allometric equations were not available for the study area, the allometric equation for moist mangrove forest stands developed by Chave et al. (2005) was used to calculate the AGB.

$$\mathrm{AGB} = 0.0509 \times \rho D^2 H \tag{1}$$

Where,

AGB = aboveground tree biomass (kg);
ρ = wood specific gravity (g cm^{-3});
D = tree diameter at breast height (DBH) (cm); and
H = tree height (m)

Table 1. Descriptive statistics of *Shorea robusta* and Other tree species.

	Shorea robusta				Other tree species			
Attributes	Mean	Min	Max	Std. Dev	Mean	Min	Max	Std. Dev
DBH (cm)	17	10	83	8.74	18	10	60	8.64
Height (m)	13	2	35	4.97	10	2	29	4.64

The AGB was then converted to carbon stock using the conversion coefficient of 0.47 as recommended by IPCC (2007) (see Equation 2). The specific wood gravity of *Shorea robusta* and Other tree species used for the estimation of AGB are 0.88 g cm^{-3} and 0.72 g cm^{-3}, respectively, as developed by ICIMOD (2010)

$$\text{Total carbon stock} = \text{Total AGB} \times 0.47 \quad (2)$$

2.5. Pre-processing of datasets

The GeoEye-1 image was available as a sensor-based rectified (OrthoReady Standard-2A) image, and it was geo-referenced to WGS 84 UTM Zone 45N projection system. Image fusion of GeoEye-1 was carried out using the 0.5 m panchromatic band and 2-m multi-spectral bands of blue, green, red, and near-infrared bands. The image fusion process resulted in a pan-sharpened multispectral image of 0.5 m spatial resolution. The first and the last returns of the airborne lidar data was used in this study, where the first return points were interpolated to a regular grid that corresponds to the digital surface model (DSM), and the last return was interpolated as digital terrain model (DTM). Each of the extracted DSM and DTM pixel size was 0.5m, and the CHM was generated by subtracting the height value of DEM from the height value of the DSM. The manually delineated tree crown polygons were overlaid on the CHM raster to extract lidar-derived tree heights and validate the tree heights.

The RapidEye image was also geo-referenced to WGS 84 UTM zone 45N projection system by taking 32 ground control points (GCPs) on RapidEye image by considering GeoEye-1 image as a reference, resulting in an overall root-mean-square error (RMSE) of 1.3 m. Atmospheric correction was applied to the georeferenced RapidEye image using ATCOR2 module in ERDAS Imagine 2010.

2.6. Image segmentation and validation

Image segmentation of the pan-sharpened MSS GeoEye image and the CHM was carried out by object-based image analysis (OBIA) technique in eCognition Developer 8.7 software. Among many image segmentation algorithms, region growing segmentation was used because it has been proven to be effective for the more complex structure of naturally regenerating forests (Erikson 2003; Ke and Quackenbush 2011b; Larsen et al. 2011). Region growing segmentation exploits spatial information and guarantees the formation of a closed connected region by aggregating pixels starting from a seed (pixel) and growing into the neighbouring pixels until a defined threshold is reached (Chen et al. 2016; Cui, Guan, and Zhang 2008). The region growing segmentation was initiated with chessboard segmentation to mask shadow and open areas, followed by detecting the local maxima and local minima. Local maxima was chosen based on the CHM layer with a filter window size of 4 × 4 pixels, as this kernel was appropriate considering the average crown diameter of 4 m in the field. A similar filter window was applied to locate the local minima. The local maxima detected as tree tops were used as a seed to initiate the region growing process and the iterative process for region growing continued until encountering a previously detected local minima. The tree crown segments were validated using the 1:1 correspondence method (Zhan et al.

2005) between manually delineated individual tree crowns and the automatic segments derived from eCognition software (Definiens 2011).

2.7. Species stratification, classification and accuracy assessment

Prior to classification, stratification of the species into two groups namely *Shorea robusta* and Other tree species was carried out based on the spectral separability curve of NIR band and the average height of the trees in each plot. From the GeoEye 1 image, the pixel values (DN) of each sample trees were extracted from the spectral profile viewer, as each profile has its own DN value in each band of the image to create a number of profiles for different types of species and the respective mean values was exported to excel sheet. The assurance of tree species' stratification was also ascertained from the Transformed Divergence technique, which estimates the probability of correct classified trees between pairs of classes. Similarly, the mean plot height of trees extracted from CHM and lidar intensity for *Shorea robusta* and Other trees was plotted and tested by one-way ANOVA for comparison of means in order to examine the differences in the tree heights between the two classes of *Shorea robusta* and Other tree species.

Therefore, the image objects were classified as *Shorea robusta* and Other trees by the nearest neighbour classification technique using the mean brightest values of NIR band from the GeoEye-1 image and the average height value of CHM for feature space optimization to ensure classification of objects with similar height and spectral attributes. The maximum layer value of bands in the feature space represents the brighter pixel of tree crowns which enables separation of different classes (Gougeon and Leckie 2006).

The training dataset comprising 70% of the identified trees on the image from the field work (296 trees) was used to train the sample tree species, while the remaining 30% was used for validating the classification result. The training dataset was used as a thematic layer to train the image objects for the classification of species. In this study, only two broad classes were classified as '*Shorea robusta*' and the 'Other tree' species because of the difficulties in species separation among different tree species. *Shorea robusta* constituted about 74% of the trees in the study area.

An error matrix was generated to evaluate the classification accuracy, and the producers and users' accuracies were calculated for each class from the error matrix. A validation dataset comprising 127 trees (96 *Shorea robusta* and 31 Other tree species) was used to assess the classification accuracy.

2.8. Statistical analysis

Regression analysis was used to model the relationship between a dependent variable (AGB as calculated from the allometric equation) and two independent variables (tree height obtained from CHM and the Crown Projection Area (CPA) from the segmented tree crowns). Individual tree crown segments which are correctly classified as *Shorea robusta* and Other tree species that have 1:1 spatial correspondence with the referenced manually delineated individual trees were used to develop the regression models. Preliminary analysis of the relationship by plotting to scatter plots between the dependent variable (aboveground carbon) and the single independent variables (height and CPA) exhibited

the non-linear relationships. Therefore, a natural logarithmic transformation was applied to both the independent and dependent variables because log transformation of the variables are recommended when the variables show skewed distribution which can be made symmetric by transforming the data (Keene 1995). Despite the non-linear relationship between a dependent variable of carbon and single independent variables of CPA and CHM height, the multiplicative log-transformed models was preferred over multiple non-linear regression in this study. It is because fitting non-linear biomass allometry models produce systematic biases in estimating biomass from small diameter trees and lead to large errors in landscape biomass estimation from a plot level dataset that is dominated by small trees (Mascaro et al. 2011).

Validation of the model performance and accuracy assessment of the estimated carbon were conducted using co-efficient of determination (R^2) for the models developed, and the RMSE. The strength and the significance of the models were validated using the partitioned 30% validation dataset. The following Equation (3) was used to calculate the RMSE.

$$\text{RMSE} = \sqrt{\frac{1}{n}\sum_{i-1}^{n}(X_0 i - X_0 i)^2} \tag{3}$$

Where,

X_o = Calculated/observed carbon;

X_p = Predicted carbon value by the model; and

n = Number of samples.

The carbon stock of the study area was calculated for the two species using the validated model as shown in Equation 4.

$$\ln Y = \beta_0 + \beta_1 \ln X_1 + \beta_2 \ln X_2 \tag{4}$$

Where,

'ln' = Natural logarithm;

Y = Aboveground carbon estimated from allometric equation;

X_1 = Height of individual trees;

X_2 = Canopy projection area (CPA) derived from automated tree segments;

β_0 = Intercept; and

β_1 & β_2 = regression coefficients for tree height and CPA, respectively.

Validated multiple regression models were used to estimate the aboveground carbon for *Shorea robusta* using the Equation 5 and for Other tree species using the Equation 6. The individual tree crown segments classified as *Shorea robusta* and Other tree species through object-based image classification and the multiple regression models as described below were used to map the aboveground carbon in the study area.

$$\ln(\text{Carbon}) = -1.70 + 1.10 \times \ln(\text{Height}) + 1.23 \times \ln(\text{CPA}) \tag{5}$$

$$\ln(\text{Carbon}) = -1.75 + 1.17 \times \ln(\text{Height}) + 1.12 \times \ln(\text{CPA}) \tag{6}$$

Where,

CPA = Canopy projection area (m^{-2}); and

Height = Height of trees (m)

2.9. Comparison of tree-centric and area-based carbon estimation

Carbon estimates for individual trees based on the model derived from CPA and height of the trees using tree-centric approach were compared to the carbon estimates at plot level, also known as area-based approach. The tree-centric carbon at plot level was estimated by aggregating the individual carbon of tree falling within the 500 m^2 of the plot (Shinzato et al. 2017), whereas area-based carbon was estimated from generalized aboveground carbon density (ACD) method suggested by (Asner & Mascaro 2014; Coomes et al. 2017) as shown in Equation 7.

$$ACD_{General} = 3.836 \times TCH^{0.281} \times BA^{0.972} \times WD^{1.376} \quad (7)$$

Where,

ACD = Aboveground carbon density;
TCH = Top canopy height (m);
BA = Basal area (m^2 (ha^{-1})), and;
WD = Wood density (gm cm^{-3})

2.10. Upscaling from reference carbon to RapidEye image

The basic idea of upscaling is to use the carbon estimates from the integration of GeoEye-1 image and lidar data in a small area as reference carbon and estimate the carbon stock at a landscape level by using a relatively coarser resolution satellite image. For upscaling, five variables were extracted from the RapidEye image to upscale the estimated carbon at the landscape level. Vegetation indices such as normalized difference vegetation index (NDVI) and RedEdge NDVI from RapidEye image was extracted using the Equations 8 and 9, respectively.

$$NDVI = \frac{(NIR - RED)}{(NIR + RED)} \quad (8)$$

Where,

NIR = Near-infrared band of RapidEye image; and
RED = Red band of RapidEye image

$$RedEdge\ NDVI = \frac{(NIR - RedEdge)}{(NIR + RedEdge)} \quad (9)$$

Where,

NIR = Near-infrared band of RapidEye image; and
RedEdge = Red edge band of RapidEye image

The principal component analysis (PCA) was performed on the image, and the first principal component (PC1) and the individual raster values of RedEdge and near-infrared (NIR) bands were also used to investigate the relationship between reference carbon and the spectral reflectance of RapidEye image. Red and NIR bands were used because these bands are sensitive to chlorophyll content in the vegetation (Wu et al. 2009) and vegetation is related to AGB.

Upscaling also known as aggregation is a process of scaling up spatial data from a finer spatial resolution image to a coarser resolution image. Among the two types of widely used aggregation techniques of categorical and numerical aggregation (Rahul, Hamm, and Kant 2013; Nelson et al. 2009; Bian and Butler 1999), the numerical aggregation technique of arithmetic sum was used to upscale the carbon estimates from integration of GeoEye-1 image and the lidar to RapidEye image. Upscaling was carried out by overlaying the reference carbon map (estimated carbon map) on the variables extracted from the RapidEye image (NDVI, RedEdge NDVI, PC1 image and the single band of red-edge and NIR bands). All the extracted variables of the RapidEye image were converted into 5 m × 5 m grids to represent the 5 m spatial resolution of RapidEye image, and each 5 m × 5 m grid contained its corresponding raster values. In both the reference carbon polygons and the converted 5 m × 5 m grids, the densities for both values were calculated, followed by the intersection of the reference carbon polygons and the 5 m × 5 m grids of RapidEye variables. The total area of the intersection was calculated, and the new carbon values inside the intersected area were calculated for each grid. The carbon values in each pixel of the RapidEye image were aggregated by summing up the total carbon of the tree crowns as a whole or parts of tree crown falling within that particular 5 m × 5 m grid of the RapidEye image. The total carbon in each 5-m pixel of the RapidEye and its corresponding raster values were extracted for further analysis. Since the dataset obtained was huge, a grid of 100 m × 100 m was created over the study area, and 10 grids were chosen randomly for further analysis. Data were partitioned into 70% and 30% as training and validation datasets, respectively. Individual tree crowns, as visualized in the VHR GeoEye-1 image and its corresponding tree crowns visualized in RapidEye imagery, are shown in Figure 2.

2.11. Relationship between up-scaled carbon and RapidEye variables

The relationship between aggregated carbon stock and the variables of RapidEye image such as NDVI, RedEdge NDVI, PC1 and the single bands of RedEdge and NIR were assessed by regression modelling. The aggregated carbon was used as a dependent

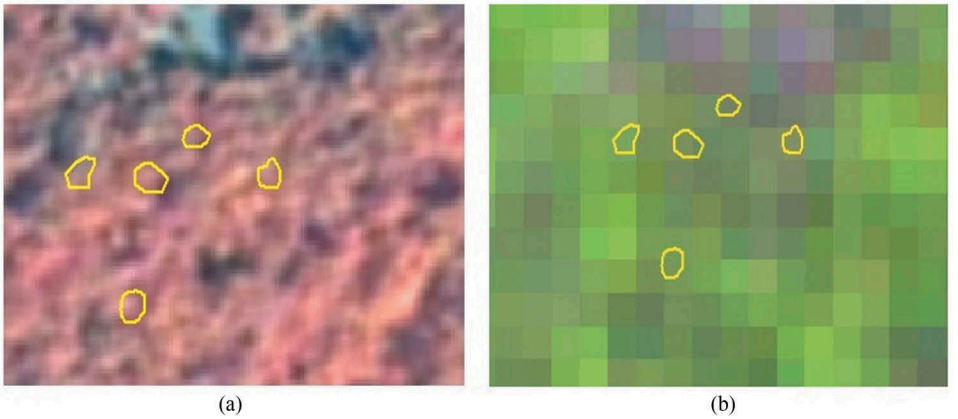

Figure 2. Yellow lines show individual tree crowns on GeoEye image (a) and RapidEye image (b).

variable and the derived vegetation indices, i.e. PC1, RedEdge band and the NIR band were used as single independent variables. The performance of the regression models was assessed by comparing the coefficient of determination (R^2) for each independent variable.

3. Results

3.1. Derivation of CHM

The CHM with a spatial resolution of 0.5 m is a three-dimensional surface that shows the vegetation height above the ground level. The field measured height as an independent variable was regressed against the CHM estimated height as a dependent variable. The coefficient of determination (R^2) was 0.75, and the correlation coefficient was 0.86 as shown in Figure 3. The relationship between the field height and the CHM height using t-test was found to be statistically significant at 95% confidence level. Comparison between the field measured height and the lidar-derived height indicated that the lidar underpredicted the actual tree heights measured in the field. There was an average underestimate of 1.1 m for the CHM tree height. The RMSE for the CHM predicted height obtained was 2.25 m with an RMSE of 13.70%. The summary statistics for the lidar-derived tree height and field measured tree height is shown in Table 2.

3.2. Species stratification

In this research, image data was segmented into *Shorea robusta* and Other tree species based on the spectral reflectance and CHM for 84 sampling plots. When the mean DN values for 5 major species were plotted on y-axis against four spectral bands on x-axis on line graph, no distinct separability of tree classes can be seen in the graph along the

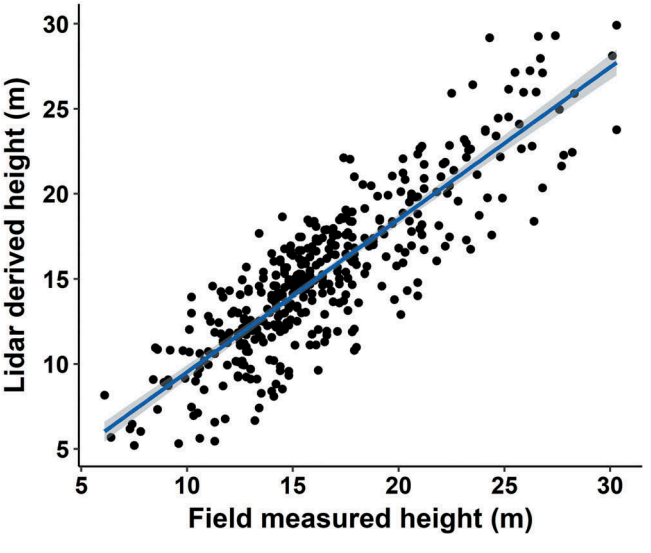

Figure 3. Scatter plot of the CHM derived height and field measured height.

Table 2. Summary statistics for the lidar derived tree height and field measured tree height.

Summary of fit	
Correlation coefficient (*r*)	0.86
R^2	0.74
Adjusted R^2	0.75
Standard Error	2.26
Root-mean-square error (RMSE)	2.25
RMSE (%)	13.70
Intercept	3.72
Slope	0.83
Number of observations	410

x-axis (bands). When the mean pixel value of *Shorea robusta* and aggregated pixel value of Other tree species was plotted on y-axis against four spectral bands on x-axis on line, a distinct separability was observed in the graph as shown in Figure 4. The spectral reflectance of *Shorea robusta* in the NIR spectral band of GeoEye-1 image was significantly different than other species. CHM of *Shorea robusta* was significantly different than the Other tree species with best average separability value of 1950.60 as calculated from transformed divergence. One-way ANOVA resulted in a highly significant difference between the mean plot height and intensity derived from lidar data with *p*-values of 0.000589 and 0.003853, respectively, which showed that these two variables are very useful in separating the tree classes at stand level as shown in Table 3.

3.3. Validation of image segmentation

Validation of the individual tree crown delineation resulted in an overall accuracy of 74% with the 1:1 correspondence method. The result showed that 313 tree crowns were only

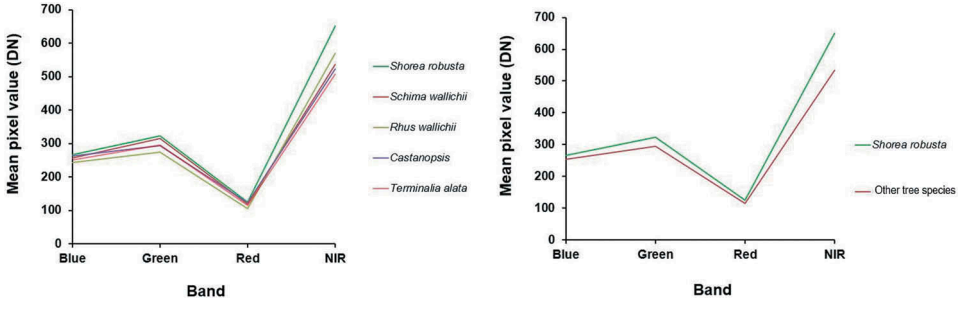

Figure 4. Spectral separability curves for individual tree species and stratified tree classes.

Table 3. One-way ANOVA for the mean plot tree height (m) and lidar intensity (points m^{-2}).

		Shorea robusta				Other tree species				
Variable	df	Min	Max	Mean	SE	Min	Max	Mean	SE	*p*-Value
Mean plot tree height	82	4.34	23.02	11.05	0.49	2.72	19.39	6.78	1.26	0.000589
Intensity	82	9.00	30.00	17.94	0.68	11.00	42.00	23.14	2.20	0.003843

matched with total number of 423 reference tree crowns and thus 74% segmentation accuracy was obtained.

3.4. Classification of tree species

Individual tree segments were classified into two main classes namely *Shorea robusta* and Other tree species using a total of 296 trees, and the accuracy assessment was carried out using the standard accuracy assessment procedure of an error matrix. The classification of trees into two main classes namely *Shorea robusta* and Other tree species produced an overall accuracy of 81.8% and a Kappa statistics value of 0.41. The accuracy matrix of the classification is shown in Table 4. The classification assessment report indicated that *Shorea robusta* was more accurately classified compared to the Other tree species with a producer's accuracy of 95.8% and user's accuracy of 82.9%.

3.5. Regression analysis

Preliminary analysis by plotting scatter diagrams for both *Shorea robusta* and Other tree species showed that the best fit was obtained using a polynomial regression between the carbon, CPA and CHM height as shown in Figures 5 and 6, respectively.

The multiple regression models for *Shorea robusta* and Other tree species revealed that the models were statistically significant at 95% confidence level using the F-test.

Table 4. Accuracy matrix for the nearest neighbour classification.

		Reference data				
		Shorea robusta	Other tree species	Total classified	Errors of commission (%)	Users' accuracy (%)
Classification	*Shorea robusta*	92	19	111	17.1	82.9
	Other tree species	4	12	16	25.0	75.0
	Total	96	31	127		
	Errors of omission (%)	4.2	61.2			
	Producers' accuracy (%)	95.8	38.8			
		Overall accuracy = 81.8%				

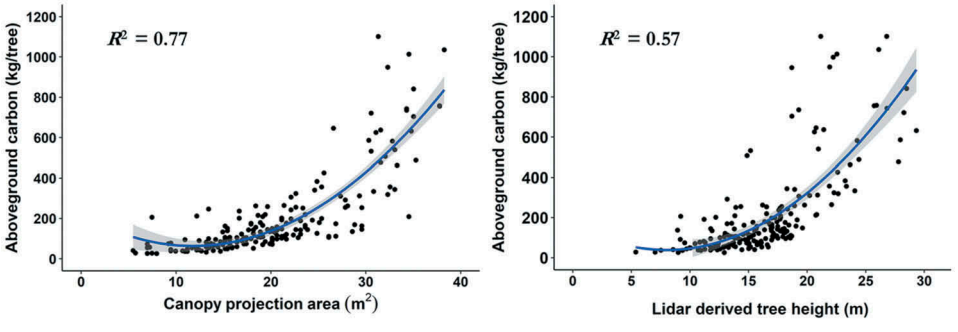

Figure 5. Scatter plots of carbon and the single independent variables for *Shorea robusta*.

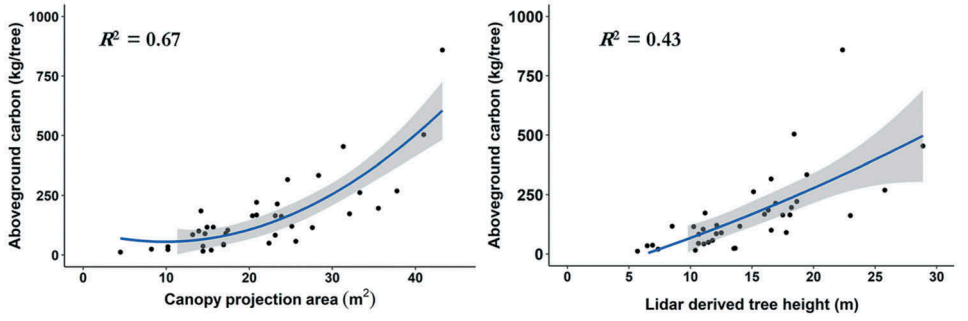

Figure 6. Scatter plots of carbon and the single independent variables for Other tree species.

The multiple regression models were validated using the 30% partitioned dataset. Observed and predicted aboveground carbon from the multiple regression models using CPA and height as an independent variable were plotted against each other. The models were validated using 85 trees (observations) in case of *Shorea robusta* and 19 trees (observations) for Other tree species. The graphical representation of the results obtained from the model validation is shown in Figure 7.

The coefficient of determination (R^2) between the observed carbon and the predicted carbon was 0.88 and 0.79 for *Shorea robusta* and Other tree species, respectively. The RMSE obtained for *Shorea robusta* was 43 kg tree^{-1} with an RMSE percent of 32% and that for the Other tree species, 44 kg tree^{-1} with an RMSE percent of 34%.

3.6. Carbon stock mapping of the study area

The carbon stock map for the study area is presented in Figure 8. The total carbon stock estimated from the multiple regression modelling for the five CF was 36,010 MgC in an area of 548 ha. The maximum carbon stock was found in Ludidamgade CF (14,014 MgC) and the lowest in Shikhar CF (3543 MgC). Despite the large area in Ludidamgade CF (271 ha), the carbon stock per area was the least amongst the five CFs, because the forests in Ludidamgade CF is a relatively young forest recovering from exposure to high deforestation.

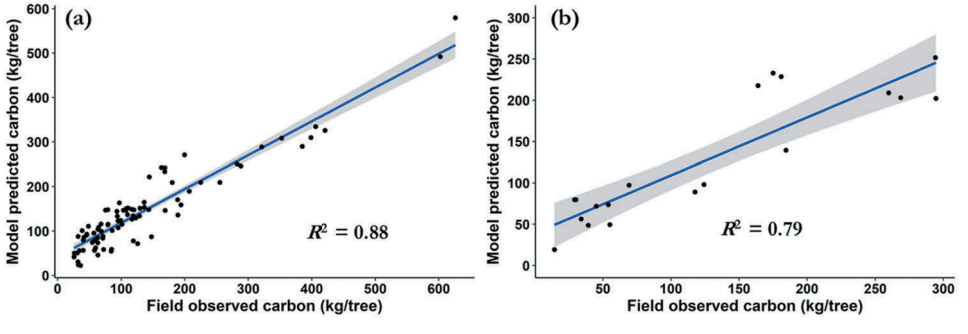

Figure 7. Scatter plots of observed and predicted carbon for *Shorea robusta* (a) and Other tree species (b).

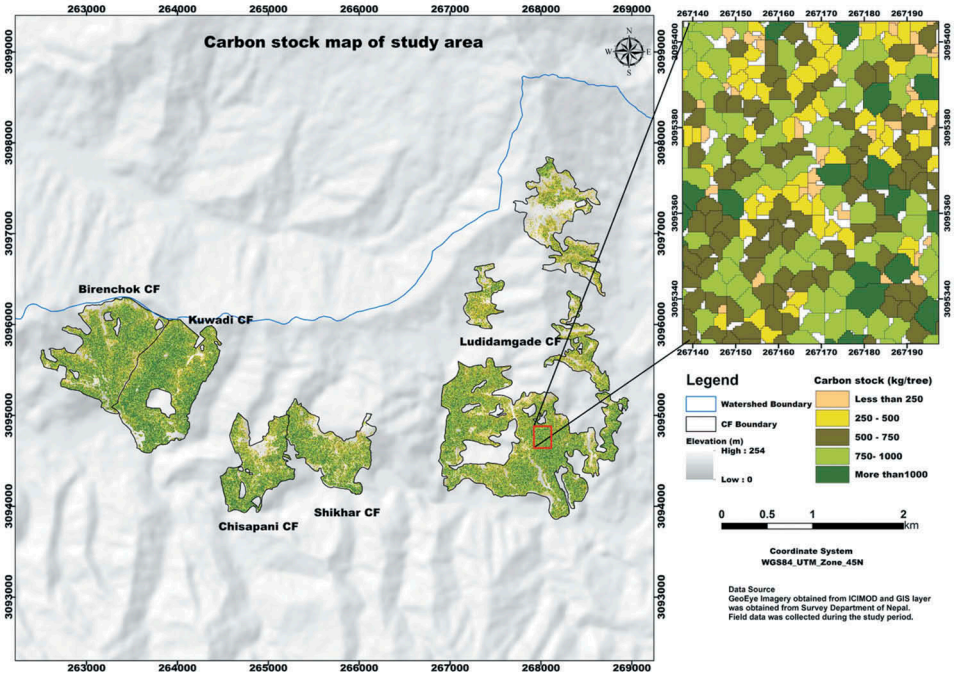

Figure 8. Carbon stock map of the study area.

3.7. Comparison of tree-centric and area-based carbon estimation

We obtained an adjusted R^2 of 0.53 between field measured carbon and the carbon estimates from ITC method and an adjusted R^2 of 0.54 between the ITC based carbon estimates and the area-based approach carbon estimates at plot level. However, higher adjusted R^2 of 0.83 was observed between the field measured carbon and the carbon estimates from area-based approach at plot level. The relationships between field measured carbon, the carbon estimates from ITC approach and carbon estimates from the area-based approaches are positively correlated and resulted with higher accuracy from ABA (RMSE = 20.04) than the ITC (Figure 9).

3.8. Upscaling of carbon derived from integration of VHR imagery and lidar data

The carbon derived from the integration of VHR GeoEye-1 image and the lidar data (both 0.5 m spatial resolution) was up-scaled by aggregating the total carbon to each 5 m pixel of RapidEye image, which consists of 100 pixels of 0.5 m resolution GeoEye-1 image.

The results obtained from upscaling the carbon polygon in 5 m pixel of RapidEye image is shown in Figure 10. Figure 10(c) shows the aggregated total carbon in each 5 m × 5 m grid.

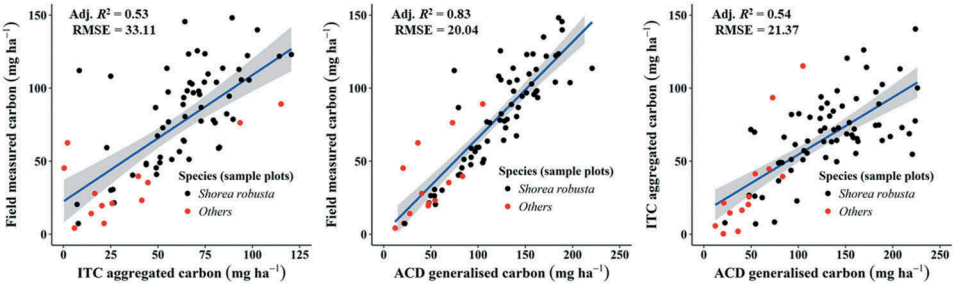

Figure 9. Scatter plots of field measured carbon, ITC and ACD carbon.

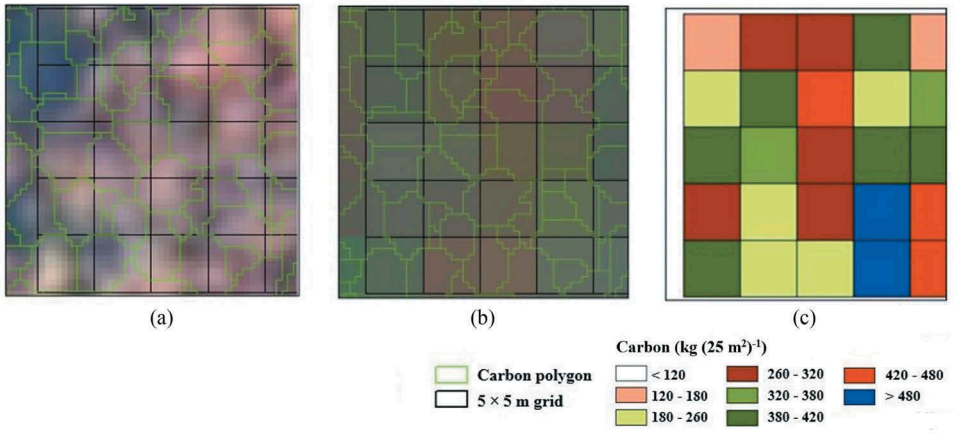

Figure 10. Upscaling from GeoEye image to RapidEye image", the label should be "Carbon polygons on GeoEye image (a) carbon polygon on RapidEye image (b) total carbon in each grid of RapidEye image (c).

3.9. Relationship between carbon and spectral reflectance of the RapidEye image

Linear regression models were used to study the relationship between the aggregated carbon and the spectral reflectance of RapidEye image variables using the 70% partitioned dataset. The results of the regression modelling using the sum carbon as the dependent variable and its corresponding variables (NDVI, RedEdge NDVI, and PC1) and the individual bands (RedEdge and NIR band) as an independent variable are shown in Table 5.

Table 5. Result from the regression modelling.

Variable	β_0	β_1	R^2	Adjusted R^2	Standard error	Number of observations
NDVI	−183.4	815.2	0.10	0.10	104.6	2126
RedEdge NDVI	−107.2	882.2	0.12	0.12	89.6	2475
PC1 component	126.7	0.10	0.18	0.17	100.1	2094
RedEdge band	892.1	−0.11	0.14	0.14	102.8	2173
NIR band	959.6	−0.09	0.11	0.11	107.9	2128

The regression models for NDVI, RedEdge NDVI, PC1, RedEdge band, and the NIR bands revealed that all the models were statistically significant at 95% confidence level. The coefficient of determination (R^2) was low for all five models. Amongst the vegetation indices and PC1, the highest R^2 obtained was 0.18 for PC1 component and the least for NDVI with an R^2 of 0.11. For the individual bands, the R^2 obtained for RedEdge band, RedEdge NDVI and NIR band was 0.14, 0.11, and 0.12, respectively. The variability of the above ground carbon explained by the spectral data is very low, as shown in Supplementary Figure 2.

Since all the developed models resulted in a low co-efficient of determination (R^2) ranging from 0.11 to 0.18, the validations of the models were not carried out. With the weak relationship between the aggregated carbon and the spectral reflectance of the RapidEye image variables, the upscaling of carbon to the 5 m spatial resolution of RapidEye image for larger areas was not carried out.

4. Discussion

This study was carried out in a complex heterogeneous forest comprising unevenly aged trees with different tree species of varied crown sizes and shapes. The CHM estimates of tree heights in this study showed an average underestimation of the ground measured tree heights by 1.1 m with an RMSE of 2.6 m. The coefficient of determination (R^2) was achieved at 0.75 and the correlation coefficient at 0.86. Heurich et al. (2004) also observed similar results of tree height underprediction by the CHM with an under-estimation of 0.42 m and an RMSE of 1.41 m in a deciduous forest stand. The high RMSE in this study is because the interpolation of lidar point clouds introduced error into the DEM, since the average lidar point sampling density used was small at 0.8 points m^{-2} and the distribution of lidar points was not homogeneous. The occurrence of three or more lidar points m^{-2} was observed in some areas, while a few areas had no points at all. Low-density lidar point cloud also causes under-estimation of the height by CHM as reported by Persson, Holmgren, and Soderman (2002). A few outliers were also found sparsely distributed over some areas which were recognized by unreasonably high elevation values in the DSM. Small footprint lidar data is helpful in estimating tree height but not recommended for individual tree height estimation.

Stratification of two species, namely *Shorea robusta* and Other tree based on spectral separability and transformed divergence values, reported a similar result as observed by Karna et al. (2015) which has almost similar forest types. Fernandes et al. (2013) also used the transformed divergence and discriminant analysis which resulted in greater spectral separability to classify temperate and the Mediterranean riparian forest with 86% accuracy. In our study, the major five tree species were tested for stratification and *Shorea robusta* showed a higher separability from other four tree species in NIR band which indicates that the GeoEye-1 image is useful for stratification of subtropical forest into two major tree classes.

The image segmentation accuracy using the region growing approach yielded an accuracy of 74% using the 1:1 spatial reference method. Erikson (2003) segmenting individual trees in a mixed forest stand reported an accuracy of 73% with the manually delineated reference tree crowns using colour infrared aerial images. Similar segmentation accuracy of 76% was also observed by Karna et al. (2015) while segmenting mixed

species tropical forest using the integrated Worldview2 image and airborne lidar data. The under segmentation was higher than over segmentation in this study, because of intermingling tree canopies, irregular tree crown shapes and peculiar branches of broadleaved tree species. When the tree crowns were intermingled, local minima were not detected due to the absence of distinct variation within the intermingled canopies. This led to under-segmentation of the individual tree crowns.

The combination of VHR imagery and the low-density lidar data improved the tree species classification than using the VHR imagery alone. The overall classification accuracy obtained in this study is 81.8%, an increase of 7.8%, higher compared to the earlier study conducted in the same area with a similar number of tree classes by Shah (2011) which resulted in an overall accuracy of 74% using the VHR satellite imagery alone. Classification accuracy increases with the combination of additional information on the vertical structure of individual trees from lidar data in addition to the spectral information from the VHR imagery. An increase in classification accuracy of 8% was also reported by Holmgren, Persson, and Soderman (2008) when integrating lidar data and high resolution aerial photograph for individual tree based classification. The increase in classification accuracy is because the lidar CHM layer mitigates the shadow effect and relief displacement which are inherent in VHR imagery.

Comparison of carbon estimates between the individual tree crown segmentation approach and the area-based approach in this study showed that the carbon estimates from individual tree crown is less accurate than the carbon estimates from area-based approach with an RMSE of 33% and 20%, respectively. Coomes et al. (2017) comparing the area-based versus tree-centric approaches to map forest carbon in the Southeast Asian forests also reported similar findings with an RMSE of 18% for individual tree carbon estimates and an RMSE of 13% for carbon estimates from area-based approach. Similar results of more accurate aboveground carbon estimates by area-based approach than the tree-centric approach is also reported by Nunes et al. (2017).

The coefficient of determination (R^2) obtained in this study is 0.74 for *Shorea robusta*, and 0.76 for Other tree species for the developed multiplicative log transformed regression models. The adjusted R^2 obtained is 0.74 and 0.75 for *Shorea robusta* and Other tree species, respectively, and the model validation showed an R^2 of 0.88 for *Shorea robusta* and 0.79 for Other tree species with an RMSE of 43 tree^{-1} for *Shorea robusta* and 44 tree^{-1} for Other tree species. The results obtained in this study agree with the findings of other studies. For instance, Lim et al. (2003a), predicting the wood volume and total aboveground biomass have obtained R^2 of 0.86 and 0.78, respectively. Their models were based on the log-transformed dependent variables of volume and biomass and the log-transformed lidar-derived height metrics in temperate deciduous hardwood forests.

In our study, a weak relationship with an R^2 of 0.18 was observed when the reference carbon estimates as a dependent variable were regressed against the PC1of RapidEye image as an independent variable. Similar weak relations were also observed between the derived carbon estimates and the NDVI and RedEdge NDVI. Previous studies have reported similar findings, stating that vegetation indices are not a good predictor of total biomass in uneven-aged and mixed broad-leaved forests (Lu et al. 2004; Sader et al. 1989; Hall, Shimabukuro, and Huemmrich 1995). Lu et al. (2004) also found a weak relationship between aboveground biomass and NDVI with a correlation coefficient (r) in the range of 0.15–0.45 in the tropical forests. The main cause of weak relationship

between the biomass and vegetation indices is the saturation of biomass in dense forest canopies. Steininger (2000) found that the canopy reflectance saturated when the biomass reached about 15 kg m^{-2} which makes biomass estimation difficult in mature forests. When saturation occurs, any further increase in biomass does not affect the values of the vegetation indices. Therefore, the vegetation indices derived from red, RedEdge and the NIR bands from RapidEye image are not suitable for establishing a relationship between carbon and spectral reflectance for upscaling to larger areas.

The relationship between the aggregated carbon and the single bands of RapidEye image (RedEdge and NIR bands) were found to be negatively linear with R^2 of 0.14 for RedEdge and 0.11 for NIR band. The R^2 value of RedEdge band was relatively higher because RedEdge band is more sensitive to vegetation than the NIR band (Wu et al. 2009). The study conducted by Lu et al. (2004) also reported similar findings with a weak negative relationship between the aboveground biomass and NIR band. The reasons for the low co-efficient of determination (R^2) between the aggregated carbon and the spectral reflectance of the RapidEye image is because the optical sensors detect only the horizontal (spatial extent) of the forest canopy and cannot detect how much biomass is found in the vertical dimensions (height) or under a canopy. The biomass in the stem that is hidden from the sensor comprises the majority of the aboveground biomass. The aboveground biomass beneath the canopy in the woody stem of a tree is estimated to comprise about 40–93% of the total biomass (Montagu et al. 2005).

Image co-registration also affected the relationship between the carbon and the spectral reflectance. The accuracy for the image to image co-registration between the VHR GeoEye-1 image and the RapidEye image was achieved with an RMSE of 1.3 m. However, there still existed some unsystematic shifts in the images. This co-registration error could have caused some discrepancies in not comparing the spectral response of the RapidEye variables with the matched carbon estimates from the integration of GeoEye-1 image and the lidar data. The temporal difference between the image acquisition dates (GeoEye-1 in November 2009 and RapidEye in April 2011) and the field data collection in October 2011 also contributed to a weak relationship between the aggregated carbon and the spectral reflectance of RapidEye image. This is because the tree crown size on the image looked slightly different from the tree crown size measured in the field.

The weakness of the relationship between the RapidEye image and the biomass/carbon stock derived from individual tree assessment could be related to the issue that this research based its assessment on individual tree approach and not on area-based approach. Coomes et al. (2017) show that selection of the approach can influence the assessment of tropical biomass/carbon. In their research, they compare the two approaches – area-based and individual tree-based. Moreover, the fact that the biomass/carbon stock was assessed based on the canopy projected area of 0.5 m resolution of GeoEye-1 image and the CHM resulted from airborne lidar data. These data carry more information about biomass/carbon stock than only a 5 m resolution of satellite MSS image of RapidEye. Therefore, RapidEye data did not show any positive relationship with the biomass/carbon stock data of the very high-resolution images and lidar data. However, the relationship could have increased if we can compare the plot level carbon as calculated from Coomes et al. (2017) with RapidEye variables as it accounted for a larger area than tree level.

Field measurement errors such as locating the exact centre of the sampling plots due to GPS error and Trupulse 360B instrument in tree height measurement could not be avoided. The strength of the signal received by the handheld GPS was weak because of cloudy weather conditions and the dense canopy of the forest structure. Difficulties in identifying the actual tree tops were also encountered due to obstruction of the actual tree tops by branches of adjoining trees. The choice of allometric equation influenced the carbon estimation models. Since the site and species-specific allometric equation for the study area was not available, the allometric equation used in this study was adapted from Chave et al. (2005), which was developed as a general allometric equation for moist mangrove forest stands. Preferably, species-specific and site-specific models should be used to reduce the errors in biomass/carbon estimation (Cairns et al. 2003).

5. Conclusion

The results of this study demonstrated the usefulness of integrating VHR satellite image and small footprint lidar data for modelling and estimating the aboveground carbon with acceptable accuracy. The significant difference of spectral separability curve extracted from GeoEye-1 image and intensity and mean plot height of the stand derived from lidar showed promising results for species stratification. This paper proposes a methodology for upscaling carbon estimates from the integration of VHR image and lidar in smaller areas to larger areas using a relatively coarser satellite image and the methodology developed in this study is expected to contribute towards the successful implementation of carbon crediting mechanisms such as REDD+ in the developing countries. However, upscaling the estimated carbon to a landscape level could not be carried out due to weak relationship between estimated carbon and the spectral reflectance of RapidEye image variables. As compared to the tree-centric approach of carbon estimation, the area-based approach for carbon estimation as proven by Coomes et al. (2017) is likely to increase the relationship of RapidEye variables and plot level carbon. For upscaling the carbon estimates derived from the tree centric approach in smaller areas to a landscape level, a cross-polarized L-band radar image of 12.5 m ALOS Pal-SAR images can be used to establish a reasonable relationship with the estimated forest biomass/carbon. Thus, upscaling could be done to even relatively coarser pixel size of 12.5 m and covers large areas. Satellite images with middle infrared (MIR) bands such as Landsat or Aster look promising too.

Acknowledgements

The authors would like to thank Himlal Shrestha and Eak Bahadur Rana from ICIMOD and B.K. Rana and Purna Magar from ANSAB for helping us during our field data collection. Thanks are also due to FRA project and Arbonaut Limited (especially Mr Basanta Gautam for addressing the reviewer's comments) for providing us with the satellite images and lidar data for this research. This research is a result of collaboration between ITC, University of Twente, Netherlands and the International Centre for Integrated Mountain Development (ICIMOD) under the REDD+ project. We also acknowledge the support of Dr Mihai A. Tanase and Dr Lauren Bennett, The University of Melbourne, for their intuitive insights to address the reviewer's comments. We would also like to thank the anonymous reviewers for their constructive comments and suggestions to improve the manuscript.

Disclosure statement

No potential conflict of interest was reported by the authors.

ORCID

Yogendra K. Karna http://orcid.org/0000-0002-2120-4710

References

Asner, G. P. 2009. "Tropical Forest Carbon Assessment: Integrating Satellite and Airborne Mapping Approaches." *Environmental Research Letters* 4 (3): 034009. doi:10.1088/1748-9326/4/3/034009.

Asner, G. P., and J. Mascaro. 2014. "Mapping Tropical Forest Carbon: Calibrating Plot Estimates to a Simple LiDAR Metric." *Remote Sensing of Environment* 140: 614–624. doi:10.1016/j.rse.2013.09.023.

Bhattarai, T., M. Skutsch, D. Midmore, and H. L. Shrestha. 2015. "Carbon Measurement: An Overview of Forest Carbon Estimation Methods and the Role of Geographical Information System and Remote Sensing Techniques for REDD+ Implementation." *Journal of Forest and Livelihood* 13 (1): 69–86. doi:10.3126/jfl.v13i1.15367.

Bian, L., and R. Butler. 1999. "Comparing Effects of Aggregation Methods on Statistical and Spatial Properties of Simulated Spatial Data." *Photogrammetric Engineering and Remote Sensing* 65: 73–84.

Brown, S. 2002. "Measuring Carbon in Forests: Current Status and Future Challenges." *Environmental Pollution* 116 (3): 363–372. doi:10.1016/s0269-7491(01)00212-3.

Cairns, M. A., I. Olmsted, J. Granados, and J. Argaez. 2003. "Composition and Aboveground Tree Biomass of a Dry Semi-Evergreen Forest on Mexico's Yucatan Peninsula." *Forest Ecology and Management* 186 (1–3): 125–132. doi:10.1016/s0378-1127(03)00229-9.

Chave, J., C. Andalo, S. Brown, M. A. Cairns, J. Q. Chambers, D. Eamus, H. Folster, et al. 2005. "Tree Allometry and Improved Estimation of Carbon Stocks and Balance in Tropical Forests." *Oecologia* 145 (1): 87–99. doi:10.1007/s00442-005-0100-x.

Chen, C. F., Y. Y. Li, C. Q. Yan, H. L. Dai, G. L. Liu, and J. Y. Guo. 2016. "An Improved Multi-Resolution Hierarchical Classification Method Based on Robust Segmentation for Filtering ALS Point Clouds." *International Journal of Remote Sensing* 37 (4): 950–968. doi:10.1080/01431161.2016.1142687.

Coomes, D. A., M. Dalponte, T. Jucker, G. P. Asner, L. F. Banin, D. F. R. P. Burslem, S. L. Lewis, et al. 2017. "Area-Based Vs Tree-Centric Approaches to Mapping Forest Carbon in Southeast Asian Forests from Airborne Laser Scanning Data." *Remote Sensing of Environment* 194 :77–88. doi:10.1016/j.rse.2017.03.017.

Cui, W., Z. Guan, and Z. Zhang. 2008. "An Improved Region Growing Algorithm for Image Segmentation." Paper presented at the 2008 International Conference on Computer Science and Software Engineering, Hubei, China, 12–14 December.

Definiens. 2011. *eCognition Developer 8.7 Reference Book*. Germany: Munchen.

Erikson, M. 2003. "Segmentation of Individual Tree Crowns in Colour Aerial Photographs Using Region Growing Supported by Fuzzy Rules." *Canadian Journal of Forest Research* 33 (8): 1557–1563. doi:10.1139/x03-062.

Fernandes, M. R., F. C. Aguiar, M. T. Ferreira, and J. M. C. Pereira. 2013. "Spectral Separability of Riparian Forests from Small and Medium-Sized Rivers across a Latitudinal Gradient Using Multispectral Imagery." *International Journal of Remote Sensing* 34 (7): 2375–2401. doi:10.1080/01431161.2012.744491.

Gautam, B. R., T. Tokola, J. Hamalainen, M. Gunia, J. Peuhkurinen, H. Parviainen, V. Leppanen, T. Kauranne, J. Havia, and I. Norjamaki. 2010. "Integration of Airborne LiDAR, Satellite Imagery, and Field Measurements Using a Two-Phase Sampling Method for Forest Biomass Estimation in

Tropical Forests". International Symposium on Benefiting from Earth Observation, 4–6 October, Kathmandu.

Gibbs, H. K., S. Brown, J. O. Niles, and J. A. Foley. 2007. "Monitoring and Estimating Tropical Forest Carbon Stocks: Making REDD a Reality." *Environmental Research Letters* 2 (4): 045023. doi:10.1088/1748-9326/2/4/045023.

Gonzalez, P., G. P. Asner, J. J. Battles, M. A. Lefsky, K. M. Waring, and M. Palace. 2010. "Forest Carbon Densities and Uncertainties from Lidar, QuickBird, and Field Measurements in California." *Remote Sensing of Environment* 114 (7): 1561–1575. doi:http://dx.doi.org/10.1016/j.rse.2010.02.011.

Gougeon, F. A., and D. G. Leckie. 2006. "The Individual Tree Crown Approach Applied to Ikonos Images of a Coniferous Plantation Area." *Photogrammetric Engineering and Remote Sensing* 72 (11): 1287–1297. doi:10.14358/PERS.72.11.1287.

Hall, F. G., Y. E. Shimabukuro, and K. F. Huemmrich. 1995. "Remote Sensing of Forest Biophysical Structure Using Mixture Decomposition and Geometric Reflectance Models." *Ecological Applications* 5 (4): 993–1013. doi:10.2307/2269350.

Heurich, M., Å. Persson, J. Holmgren, and E. Kennel. 2004. "Detecting and Measuring Individual Trees with Laser Scanning in Mixed Mountain Forest of Central Europe Using an Algorithm Developed for Swedish Boreal Forest Conditions." *International Archives of Photogrammetry, Remote Sensing and Spatial Information Sciences* 36: 307–312.

Holmgren, J., A. Persson, and U. Soderman. 2008. "Species Identification of Individual Trees by Combining High Resolution LIDAR Data with Multi-Spectral Images." *International Journal of Remote Sensing* 29 (5): 1537–1552. doi:10.1080/01431160701736471.

Hou, Z., X. Qing, and T. Tokola. 2011. "Use of ALS, Airborne CIR and ALOS AVNIR-2 Data for Estimating Tropical Forest Attributes in Lao PDR." *Isprs Journal of Photogrammetry and Remote Sensing* 66 (6): 776–786. doi:10.1016/j.isprsjprs.2011.09.005.

Husch, B., T. W. Beers, and J. A. Kershaw. 2003. *Forest Mensuration*. Wiley Blackwell.

ICIMOD. 2010. "Forest Carbon Stock in REDD+ Pilot Project Sites: Year One Measurement & Analysis". Accessed 15 Nov. http://communityredd.net/userfiles/Nepal%20REDD%20CStock%20Year%20One%20Report%202010.pdf

IPCC. 2007. *Climate Change 2007, Synthesis Report. Contribution of Working Groups I, II and III to the Fourth Assessment Report of the Intergovernmental Panel on Climate Change*, edited by Core Writing Team, R. K. Pachauri and A. Reisinger, 104. Geneva, Switzerland: IPCC.

Johansen, K., N. C. Coops, S. E. Gergel, and Y. Stange. 2007. "Application of High Spatial Resolution Satellite Imagery for Riparian and Forest Ecosystem Classification." *Remote Sensing of Environment* 110 (1): 29–44. doi:10.1016/j.rse.2007.02.014.

Joseph, M. H., W. D. Sunderlin, and L. V. Verchot. 2013. "REDDC Readiness: Early Insights on Monitoring, Reporting and Verification Systems of Project Developers." *Environment Research Letters* 8. doi:10.1088/1748-9326/8/3/034038.

Karna, Y. K., Y. A. Hussin, H. Gilani, M. C. Bronsveld, M. S. R. Murthy, F. M. Qamer, B. S. Karky, T. Bhattarai, X. Aigong, and C. B. Baniya. 2015. "Integration of WorldView-2 and Airborne LiDAR Data for Tree Species Level Carbon Stock Mapping in Kayar Khola Watershed, Nepal." *International Journal of Applied Earth Observation and Geoinformation* 38: 280–291. doi:10.1016/j.jag.2015.01.011.

Ke, Y. H., and L. J. Quackenbush. 2011a. "A Review of Methods for Automatic Individual Tree-Crown Detection and Delineation from Passive Remote Sensing." *International Journal of Remote Sensing* 1–23. doi:10.1080/01431161.2010.494184.

Ke, Y. H., L. J. Quackenbush, and J. Im. 2010. "Synergistic Use of QuickBird Multispectral Imagery and LIDAR Data for Object-Based Forest Species Classification." *Remote Sensing of Environment* 114 (6): 1141–1154. doi:10.1016/j.rse.2010.01.002.

Ke, Y., and L. J. Quackenbush. 2011b. "A Comparison of Three Methods for Automatic Tree Crown Detection and Delineation from High Spatial Resolution Imagery." *International Journal of Remote Sensing* 32 (13): 3625–3647. doi:10.1080/01431161003762355.

Keene, O. N. 1995. "The Log Transformation Is Special." *Statistics in Medicine* 14 (8): 811–819.

Larsen, M., M. Eriksson, X. Descombes, G. Perrin, T. Brandtberg, and F. A. Gougeon. 2011. "Comparison of Six Individual Tree Crown Detection Algorithms Evaluated under Varying Forest Conditions." *International Journal of Remote Sensing* 1–26. doi:10.1080/01431161.2010.507790.

Latifi, H., F. E. Fassnacht, F. Hartig, C. Berger, J. Hernández, P. Corvalán, and B. Koch. 2015. "Stratified Aboveground Forest Biomass Estimation by Remote Sensing Data." *International Journal of Applied Earth Observation and Geoinformation* 38: 229–241. doi:10.1016/j.jag.2015.01.016.

Leboeuf, A., A. Beaudoin, R. A. Fournier, L. Guindon, J. E. Luther, and M. C. Lambert. 2007. "A Shadow Fraction Method for Mapping Biomass of Northern Boreal Black Spruce Forests Using QuickBird Imagery." *Remote Sensing of Environment* 110 (4): 488–500. doi:10.1016/j.rse.2006.05.025.

Leckie, D. G., F. Gougeon, D. Hill, R. Quinn, L. Armstrong, and R. Shreenan. 2003. "Combined High-Density Lidar and Multispectral Imagery for Individual Tree Crown Analysis." *Canadian Journal of Remote Sensing* 29 (5): 633–649. doi:10.5589/m03-024.

Lefsky, M. A., W. B. Cohen, S. A. Acker, G. G. Parker, T. A. Spies, and D. Harding. 1999a. "Lidar Remote Sensing of the Canopy Structure and Biophysical Properties of Douglas-Fir Western Hemlock Forests." *Remote Sensing of Environment* 70 (3): 339–361. doi:10.1016/s0034-4257(99)00052-8.

Lefsky, M. A., W. B. Cohen, and T. A. Spies. 2001. "An Evaluation of Alternate Remote Sensing Products for Forest Inventory, Monitoring, and Mapping of Douglas-Fir Forests in Western Oregon." *Canadian Journal of Forest Research-Revue Canadienne De Recherche Forestiere* 31 (1): 78–87. doi:10.1139/cjfr-31-1-78.

Lim, K., P. Treitz, K. Baldwin, I. Morrison, and J. Green. 2003a. "Lidar Remote Sensing of Biophysical Properties of Tolerant Northern Hardwood Forests." *Canadian Journal of Remote Sensing* 29 (5): 658–678. doi:10.5589/m03-025.

Lin, W., Y. Meng, Z. Qiu, S. Zhang, and W. Jinzhuo. 2017. "Measurement and Calculation of Crown Projection Area and Crown Volume of Individual Trees Based on 3D Laser-Scanned Point-Cloud Data." *International Journal of Remote Sensing* 38 (4): 1083–1100. doi:10.1080/01431161.2016.1265690.

Lou, S., C. Wang, X. Xiaohuan, F. Pan, D. Peng, J. Zou, S. Nie, and H. Qin. 2016. "Fusion of Airborne LiDAR Data and Hyperspectral Imagery for Aboveground and Belowground Forest Biomass Estimation." *Ecological Indicators* 73 (2017): 378–387.

Lu, D., P. Mausel, E. Brondizio, and E. Moran. 2004. "Relationships between Forest Stand Parameters and Landsat TM Spectral Responses in the Brazilian Amazon Basin." *Forest Ecology and Management* 198 (1–3): 149–167. doi:10.1016/j.foreco.2004.03.048.

Lu, D. S. 2006. "The Potential and Challenge of Remote Sensing-Based Biomass Estimation." *International Journal of Remote Sensing* 27 (7): 1297–1328. doi:10.1080/01431160500486732.

Mascaro, J., C. M. Litton, R. Flint Hughes, A. Uowolo, and S. A. Schnitzer. 2011. "Minimizing Bias in Biomass Allometry: Model Selection and Log-Transformation of Data." *Biotropica* 43 (6): 649–653. doi:10.1111/j.1744-7429.2011.00798.x.

MFSC. 2018. "REDD Implementation Center". MFSC, Accessed 12 Mar 2018. http://mofsc-redd.gov.np/resource-center/

Montagu, K. D., K. Düttmer, C. V. M. Barton, and A. L. Cowie. 2005. "Developing General Allometric Relationships for Regional Estimates of Carbon Sequestration—An Example Using Eucalyptus Pilularis from Seven Contrasting Sites." *Forest Ecology and Management* 204 (1): 115–129. doi:10.1016/j.foreco.2004.09.003.

Muukkonen, P., and J. Heiskanen. 2007. "Biomass Estimation over A Large Area Based on Standwise Forest Inventory Data and ASTER and MODIS Satellite Data: A Possibility to Verify Carbon Inventories." *Remote Sensing of Environment* 107 (4): 617–624. doi:10.1016/j.rse.2006.10.011.

Naesset, E. 2011. "Estimating Above-Ground Biomass in Young Forests with Airborne Laser Scanning." *International Journal of Remote Sensing* 32 (2): 473–501. doi:10.1080/01431160903474970.

Nelson, M. D., R. E. McRoberts, G. R. Holden, and M. E. Bauer. 2009. "Effects of Satellite Image Spatial Aggregation and Resolution on Estimates of Forest Land Area." *International Journal of Remote Sensing* 30 (8): 1913–1940. doi:10.1080/01431160802545631.

Nunes, M. H., R. M. Ewers, E. C. Turner, and D. A. Coomes. 2017. "Mapping Aboveground Carbon in Oil Palm Plantations Using LiDAR: A Comparison of Tree-Centric versus Area-Based Approaches." *Remote Sensing* 9: 8. doi:10.3390/rs9080816.

Omasa, K., G. Y. Qiu, K. Watanuki, K. Yoshimi, and Y. Akiyama. 2003. "Accurate Estimation of Forest Carbon Stocks by 3-D Remote Sensing of Individual Trees." *Environmental Science & Technology* 37 (6): 1198–1201. doi:10.1021/es0259887.

Patenaude, G., R. A. Hill, R. Milne, D. L. A. Gaveau, B. B. J. Briggs, and T. P. Dawson. 2004. "Quantifying Forest above Ground Carbon Content Using LiDAR Remote Sensing." *Remote Sensing of Environment* 93 (3): 368–380. doi:10.1016/j.rse.2004.07.016.

Patenaude, G., R. Milne, and T. P. Dawson. 2005. "Synthesis of Remote Sensing Approaches for Forest Carbon Estimation: Reporting to the Kyoto Protocol." *Environmental Science & Policy* 8 (2): 161–178. doi:10.1016/j.envsci.2004.12.010.

Persson, Å., J. Holmgren, and U. Soderman. 2002. "Detecting and Measuring Individual Trees Using an Airborne Laser Scanner." *Photogrammetric Engineering and Remote Sensing* 68 (9): 925–932.

Popescu, S. C. 2007. "Estimating Biomass of Individual Pine Trees Using Airborne Lidar." *Biomass & Bioenergy* 31 (9): 646–655. doi:10.1016/j.biombioe.2007.06.022.

Popescu, S. C., R. H. Wynne, and J. A. Scrivani. 2004. "Fusion of Small-Footprint Lidar and Multispectral Data to Estimate Plot-Level Volume and Biomass in Deciduous and Pine Forests in Virginia, USA." *Forest Science* 50 (4): 551–565.

Rahul, R., N. A. S. Hamm, and Y. Kant. 2013. "Analysing the Effect of Different Aggregation Approaches on Remotely Sensed Data." *International Journal of Remote Sensing* 34 (14): 4900–4916. doi:10.1080/01431161.2013.781289.

Rana, P., L. Korhonen, B. Gautam, and T. Tokola. 2014. "Effect of Field Plot Location on Estimating Tropical Forest Above-Ground Biomass in Nepal Using Airborne Laser Scanning Data." *Isprs Journal of Photogrammetry and Remote Sensing* 94: 55–62. doi:10.1016/j.isprsjprs.2014.04.012.

Sader, S. A., R. B. Waide, W. T. Lawrence, and A. T. Joyce. 1989. "Tropical Forest Biomass and Successional Age Class Relationships to a Vegetation Index Derived from Landsat TM Data." *Remote Sensing of Environment* 28: 143–198. doi:10.1016/0034-4257(89)90112-0.

Sexton, J. O., T. Bax, P. Siqueira, J. J. Swenson, and S. Hensley. 2009. "A Comparison of Lidar, Radar, and Field Measurements of Canopy Height in Pine and Hardwood Forests of Southeastern North America." *Forest Ecology and Management* 257 (3): 1136–1147. doi:10.1016/j.foreco.2008.11.022.

Shah, R. 2011. "Comparison of Individual Tree Crown Delineation Methods for Carbon Stock Estimation Using Very High Resolution Satellite Images". Unpublished MSc Thesis, University of Twente Faculty of Geo-Information and Earth Observation ITC.

Shi, L., and S. Liu. 2017. "Methods of Estimating Forest Biomass: A Review." In *Biomass Volume Estimation and Valorization for Energy*, edited by J. S. Tumuluru, 23–46. London: InTechOpen. doi: 10.5772/65733.

Shinzato, E. T., Y. E. Shimabukuro, N. C. Coops, P. Tompalski, and E. A. G. Gasparoto. 2017. "Integrating Area-Based and Individual Tree Detection Approaches for Estimating Tree Volume in Plantation Inventory Using Aerial Image and Airborne Laser Scanning Data." *Iforest-Biogeosciences and Forestry* 10: 296–302. doi:10.3832/ifor1880-009.

Song, C., M. B. Dickinson, S. Lihong, S. Zhang, and D. Yaussey. 2010. "Estimating Average Tree Crown Size Using Spatial Information from Ikonos and QuickBird Images: Across-Sensor and Across-Site Comparisons." *Remote Sensing of Environment* 114 (5): 1099–1107. doi:10.1016/j.rse.2009.12.022.

Steininger, M. K. 2000. "Satellite Estimation of Tropical Secondary Forest Above-Ground Biomass: Data from Brazil and Bolivia." *International Journal of Remote Sensing* 21 (6–7): 1139–1157. doi:10.1080/014311600210119.

UNEP. 2011. "UNEP-About the UN-REDD Programme". Accessed 29 May. http://www.unep.org/climatechange/reddplus/Home/tabid/29506/Default.aspx

UN-REDD. 2011. "UN Collaborative Programme on Reducing Emissions from Deforestation and Forest Degradation in Developing Countries (UN-REDD) Framework Document". Accessed 26 May. http://www.fao.org/climatechange/unredd/53079/en/

Wu, C., Z. Niu, Q. Tang, W. Huang, B. Rivard, and J. Feng. 2009. "Remote Estimation of Gross Primary Production in Wheat Using Chlorophyll-Related Vegetation Indices." *Agricultural and Forest Meteorology* 149 (6–7): 1015–1021. doi:10.1016/j.agrformet.2008.12.007.

Yin, D. M., and L. Wang. 2016. "How to Assess the Accuracy of the Individual Tree-Based Forest Inventory Derived from Remotely Sensed Data: A Review." *International Journal of Remote Sensing* 37 (19): 4521–4553. doi:10.1080/01431161.2016.1214302.

Zhan, Q., M. Molenaar, K. Tempfli, and W. Shi. 2005. "Quality Assessment for Geo-Spatial Objects Derived from Remotely Sensed Data." *International Journal of Remote Sensing* 26 (14): 2953–2974. doi:10.1080/01431160500057764.

Zheng, D., J. Rademacher, J. Chen, T. Crow, M. Bresee, J. Le Moine, and S.-R. Ryu. 2004. "Estimating Aboveground Biomass Using Landsat 7 ETM+ Data across a Managed Landscape in Northern Wisconsin, USA." *Remote Sensing of Environment* 93 (3): 402–411. doi:10.1016/j.rse.2004.08.008.